

# Proximity effect at superconducting Sn-Bi<sub>2</sub>Se<sub>3</sub> interface

Fan Yang,<sup>1</sup> Yue Ding,<sup>1</sup> Fanming Qu,<sup>1</sup> Jie Shen,<sup>1</sup> Jun Chen,<sup>1</sup> Zhongchao Wei,<sup>1</sup>  
Zhongqing Ji,<sup>1</sup> Guangtong Liu,<sup>1</sup> Jie Fan,<sup>1</sup> Changli Yang,<sup>1</sup> Tao Xiang,<sup>1,2</sup> and Li Lu<sup>1,\*</sup>

<sup>1</sup>*Daniel Chee Tsui Laboratory, Beijing National Laboratory for Condensed Matter Physics,  
Institute of Physics, Chinese Academy of Sciences, Beijing 100190, China*

<sup>2</sup>*Institute of Theoretical Physics, Chinese Academy of Sciences, Beijing 100190, China*  
(Dated: November 7, 2018)

We have investigated the conductance spectra of Sn-Bi<sub>2</sub>Se<sub>3</sub> interface junctions down to 250 mK and in different magnetic fields. A number of conductance anomalies were observed below the superconducting transition temperature of Sn, including a small gap different from that of Sn, and a zero-bias conductance peak growing up at lower temperatures. We discussed the possible origins of the smaller gap and the zero-bias conductance peak. These phenomena support that a proximity-effect-induced chiral superconducting phase is formed at the interface between the superconducting Sn and the strong spin-orbit coupling material Bi<sub>2</sub>Se<sub>3</sub>.

PACS numbers: 74.45.+c, 03.65.Vf, 71.70.Ej, 73.40.-c

## I. INTRODUCTION

Due to strong spin-orbit coupling (SOC), electrons in the surface states (SS) of a topological insulator (TI) become completely helical, forming a new category of half metals<sup>1-3</sup>. Among many exciting features of TIs, the exotic physics at the interface between a three-dimensional (3D) TI and an *s*-wave superconductor is of particular interest. According to theoretical predictions, novel superconductivity with effectively spinless  $p_x + ip_y$  pairing symmetry will be induced via proximity effect, and Majorana bound states will emerge at the edges<sup>4-8</sup>. Several experimental schemes have been proposed to test the predictions, but the progresses so far reported are limited to the observations of a supercurrent in Al-Bi<sub>2</sub>Se<sub>3</sub>-Al junctions<sup>9</sup>. It is not clear whether this is because the predicted exotic properties are suppressed by the existence of bulk states (BS) which are present in most transport measurements. Nevertheless, there are signs that the majority electrons are still significantly helical in the presence of BS. For example, the magnetoresistance of Bi<sub>2</sub>Se<sub>3</sub> exhibits an unusually robust weak anti-localization behavior<sup>10-14</sup>, indicating the existence of a Berry phase  $\pi$  in the band structure of those electrons involved in transport measurements. Therefore, it is possible that some of the novel properties originally predicated for ideal TIs are still experimentally observable even in the presence of BS.

In this Article, we report our experimental investigation on the conductance spectra of superconductor-normal metal (S-N) interface junctions made of Sn film and Bi<sub>2</sub>Se<sub>3</sub> single crystalline flake with BS, where Sn is a simple *s*-wave superconductor, and Bi<sub>2</sub>Se<sub>3</sub> is a typical 3D TI candidate<sup>15</sup>. Several anomalies were found, including a double-gap structure that develops below the superconducting transition temperature of Sn and a zero-bias conductance peak grown up at lower temperatures. We will discuss the possible origins of these phenomena, and to show that they can be interpreted by the formation of

a proximity-effect-induced chiral superconducting phase at the interface.

## II. EXPERIMENT: Sn-Bi<sub>2</sub>Se<sub>3</sub> JUNCTIONS

The Bi<sub>2</sub>Se<sub>3</sub> flakes used in this experiment were mechanically exfoliated from a high quality single crystal, and those with thickness of  $\sim 100$  nm were transferred to degenerate-doped Si substrates with a 300 nm-thick SiO<sub>2</sub> for device fabrication. Two Pd electrodes were firstly deposited to a selected flake. Then, an insulating layer of heavily-overexposed PMMA photoresist with a  $1 \times 1 \mu\text{m}^2$  hole at the center was fabricated on top of the flake. Finally, 200-nm-thick Sn electrodes were patterned and deposited via sputtering. The device structure and measurement configuration are illustrated in Figs. 1(b) and 1(c). Pseudo-four-terminal measurement was performed in a <sup>3</sup>He cryostat by using lock-in amplifiers, with an ac excitation current of 1  $\mu\text{A}$  at 30.9 Hz.

Determined from Hall effect measurements, the thin flakes of Bi<sub>2</sub>Se<sub>3</sub> used in this experiment have a typical carrier density of  $10^{18} \text{ cm}^{-3}$  and a typical mobility of  $5000 \text{ cm}^2/\text{Vs}$  at  $T = 1.6 \text{ K}$ . The Sn films deposited show a sharp superconducting transition at  $T_c \approx 3.8 \text{ K}$  and with a critical field  $H_c$  less than 60 mT at 300 mK, indicating their high quality in term of superconductivity, in spite of the granular morphology [Fig. 1(c)] due to self-annealing at room temperature.

For the study of proximity effect, a clean interface and a relatively small junction resistance are necessary. If the interfacial barrier strength is too high, no proximity effect will occur. In order to improve the contact between Sn and Bi<sub>2</sub>Se<sub>3</sub>, some of the devices were treated with Ar ion etching in a reacting ion etching system, to remove the possible remnant photoresist in the junction area prior to Sn deposition (with a pressure of 100 mTorr, a power of 50 W and for  $\sim 10$  s). Since Ar does not react with Bi<sub>2</sub>Se<sub>3</sub>, the etching is generally a physical process. Ar etching is found to be helpful to enhance the trans-

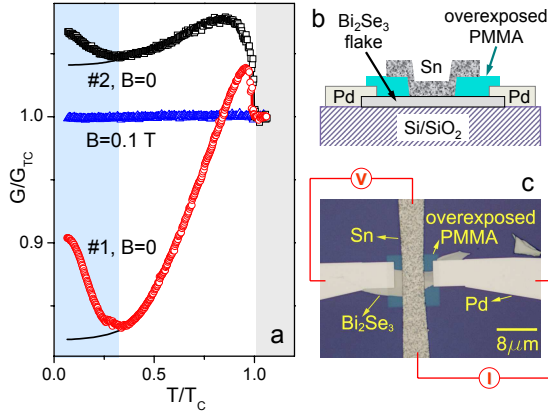


FIG. 1: (color online) (a) Temperature dependencies of zero-bias conductance of Sn-Bi<sub>2</sub>Se<sub>3</sub> junction devices #1 and #2. The temperature is normalized to the superconducting transition point of the Sn film,  $T_c \approx 3.8$  K, and the conductance is normalized to its value just above  $T_c$ . The solid lines represent the tendency of saturation expected from BTK theory for  $s$ -wave S-N junctions with a medium interfacial scattering strength<sup>16</sup>. A magnetic field of 0.1 T completely suppressed all the features below  $T_c$ . The white and blue regions correspond to the two stages of proximity effect discussed in the text. (b) Illustrations of the device structure. (c) Optical image of the device and measurement configuration.

parency of the junction. But good contact can still be

achieved without etching. The primary features of the conductance spectra were found to be similar for devices with comparable interfacial resistance, regardless of the treatment prior to Sn deposition.

More than a dozen devices were fabricated and measured at  $T=1.6$  K, six of them were further investigated down to 250 mK. All devices exhibited qualitatively similar features. In this Article, we show the data taken from three typical devices, labeled as #1, #2 and #3. The normal-state resistance (taken at  $T = 4$  K) of these devices are 13.5  $\Omega$ , 7.5  $\Omega$  and 10.2  $\Omega$ , respectively.

Figure 1(a) shows the measured zero-bias differential conductance  $G$  as a function of  $T$  for device #1 and #2, where the data are normalized to their values above  $T_c \approx 3.8$  K. With decreasing  $T$ , the conductance increases abruptly below  $T_c$ , and reaches a peak with a maximum enhancement of 3.9% for device #1 and 7.7% for device #2, then the conductance drops gradually until a turning point  $\sim 1.2$  K. Below this temperature, the conductance increases and deviating from the saturation tendency expected from the BTK theory<sup>16</sup>. The deviation at 250 mK is  $\sim 8\%$  for devices #1 and  $\sim 3\%$  for devices #2. By applying a magnetic field  $B=0.1$  T, all the low-temperature structures on the  $G-T$  curves were removed, indicating that they are closely related to the superconductivity of Sn.

In BTK theory<sup>16</sup>, the normalized zero-bias  $dI/dV$  of an S-N junction,  $Y$ , can be written as:

$$Y(Z, T) = \frac{I_{NS}(Z, T)}{I_{NN}(Z)} \Big|_{eV \rightarrow 0} = (1 + Z^2) \int_{-\infty}^{\infty} \left( \frac{\partial f_0}{\partial E} \right) [2A(E) + C(E) + D(E)]$$

where the dimensionless parameter  $Z$  describes the barrier strength of the S-N junction,  $f_0(E, T)$  is the Fermi distribution,  $A(E)$ ,  $C(E)$  and  $D(E)$  are functions defined in the BTK theory. At  $T = 0$  this equation can be simplified to:

$$Y|_{T=0} = \frac{2(1 + Z^2)}{(1 + 2Z^2)^2}$$

With this formula, one can estimate the  $Z$  value of a device using its saturated conductance at low temperatures.

In Fig. 1(a), the normalized  $dI/dV$  for devices #1 and #2 saturate to about 0.82 and 1.04, as indicated by the solid lines, which yield barrier strengths of  $Z = 0.66$  and 0.54 for devices #1 and #2, respectively. Such barriers are not in the transparent limit (i.e.,  $Z = 0$ ) nor in the tunneling limit ( $Z \gg 1$ ), which ensures the happening of reasonably strong proximity effect at the interface on one hand, and enabling us to probe the information of the density of states on the other hand.

In Fig. 2 and Fig. 3 we show the conductance spectra, namely the bias voltage ( $V_{\text{bias}}$ ) dependence of differential conductance, of device #1 measured at different temperatures and in different magnetic fields. Each curve is normalized to its high bias value in region III. Three unusual features were observed, as elaborated below.

The first feature is a bump-like enhancement, together with sharp dips at the two sides. It develops at temperatures immediately below  $T_c$  in regions I and II, as marked in Fig. (2), and is best seen at high  $T$  when the gaps are largely undeveloped. It corresponds to the abrupt increase of conductance in the  $G-T$  curves just below  $T_c$ . With decreasing  $T$  the bump structure evolves and extends to a bias voltage several times larger than the superconducting gap of Sn. In the mean time gap structures develop around zero bias voltage, which will be discussed later.

The position of the dips is device-dependent. It is very close to zero bias voltage at temperatures just below  $T_c$ , but can reach as high as 8 mV at low temperatures for high resistance junctions in this experiment (data not

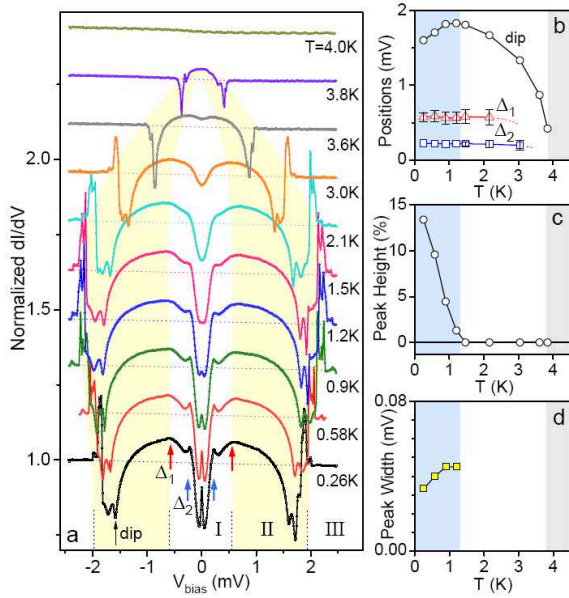


FIG. 2: (color online) (a) Conductance spectra of device #1 at different temperatures. Each curve is normalized to its high bias value, and is shifted vertically for clarity. (b) Temperature dependencies of the positions of the dip, the first gap  $\Delta_1$ , and the second gap  $\Delta_2$ . (c) Temperature dependence of the peak height. The peak grows up at a temperature significantly lower than the  $T_c$  of Sn. (d) Temperature dependence of the full width of the peak at half height.

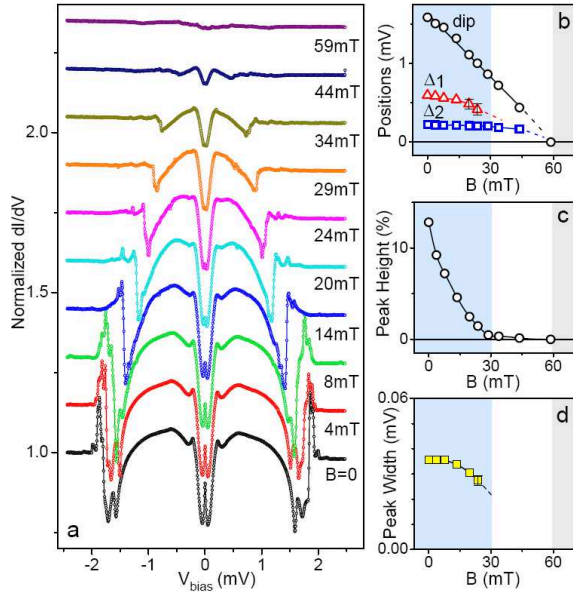


FIG. 3: (color online) (a) Conductance spectra of device #1 taken at 300 mK and in different magnetic fields. Curves have been shifted vertically for clarity. (b) Field dependencies of the positions of the dip, the first gap  $\Delta_1$ , and the second gap  $\Delta_2$ . (c) Field dependence of the peak height. (d) Field dependence of the full width of the peak at half height.

shown). The dips can be safely attributed to current-driven destruction of superconductivity in the local Sn film surrounding the junction. We note that the use of large measurement current (up to 200  $\mu\text{A}$  here) is unavoidable in proximity effect studies where the junctions usually need to be reasonably transparent. Estimation shows that the local current density at the step edge of the window of our junctions could reach to  $\sim 10^4$  to  $10^5$   $\text{A}/\text{cm}^2$  at  $V_{\text{bias}}=2$  mV (for a 10  $\Omega$  junction), which may well exceed the critical current density of the Sn film. The non-monotonic  $T$  dependence of the dip position, as shown in Fig. 2, Fig. 4 for devices #1 and #3, and in Fig. 7 for comparative Sn-graphite devices, suggests that the detailed destruction process might involve local heating and thermal conduction which has a significant temperature dependence below  $\sim 1$  K (see Section III).

The second feature in the conductance spectra is a double-gap structure that develops on the enhanced conductance background, as shown in region I of Fig. 2(a). The borders of the two gaps are indicated by the arrows. The development of this structure is responsible for the drop of  $G-T$  curves below the peak temperatures in Fig. 1(a). For device #1, the first (bigger) gap is  $\Delta_1=0.59$  mV, which matches with the superconducting gap of Sn, and the second (smaller) gap is  $\Delta_2=0.21$  mV, only about 1/3 of the first one. It should be noted that for most devices (10 out of 12) only the smaller gap was clearly observed. In Figs. 4(a) and 4(d) we show two such examples observed on devices #3 and #2, respectively. For device #3, a faint structure can still be resolved at the  $\Delta_1$  position, as indicated by the blue arrows in Fig. 4(a), and is best seen on the curve taken at 1.2 K.

The existence of two distinct gaps clearly indicates that the smaller gap is not the superconducting gap of Sn. It should arise from some new superconducting phase formed at the interface, which will be further discussed later.

The third feature in the conductance spectra is a zero bias conductance peak (ZBCP) developed at low temperatures. This ZBCP is responsible for the conductance increment on  $G-T$  curves below  $\sim 1.2$  K. The peak height grows up almost linearly with decreasing  $T$ . It reaches 13.4% and 16.4% of the normal-state conductance at the lowest temperature of this experiment, 250 mK, for device #1 and #3 respectively, as shown in Figs. 2(c) and 4(b). And the peak width<sup>18</sup> decreases with decreasing  $T$  at low temperatures, as shown in Figs. 2(d) and 4(c). Both the height and the width of the ZBCP can be suppressed by applying a magnetic field, as shown in Figs. 3(c) and 3(d).

The temperature dependence of peak width contains important information about the origin of the ZBCP. When we plot the ZBCP against bias current instead of bias voltage, as shown in Figs. 5(a) and 5(b) for devices #1 and #3 respectively, the peak width decreases with decreasing  $T$  as well [Fig. 5(c)]. It indicates that the ZBCP is originated from some kind of resonance whose

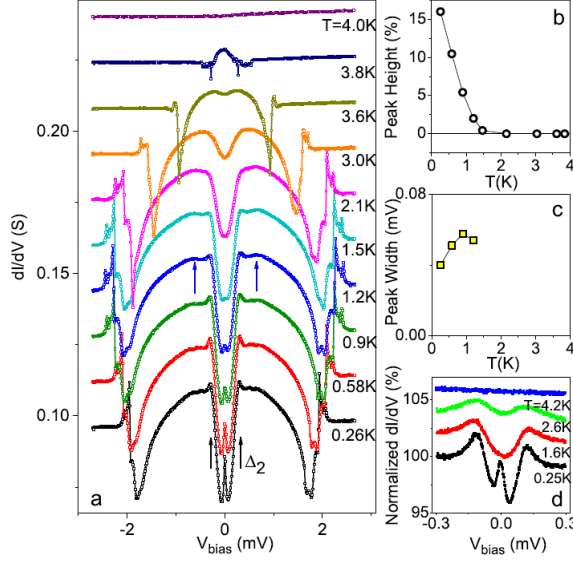


FIG. 4: (color online) (a) Conductance spectra of device #3 taken in zero magnetic field and at different temperatures. The blue arrows indicate where the coherence peak of the bigger gap  $\Delta_1$  is expected. Only a faint structure at this position can be resolved (which is best seen on the 1.2 K curve). Curves have been shifted vertically for clarity. (b) Temperature dependence of the peak height at zero bias voltage. (c) Temperature dependence of the full width of the peak at half height. (d) Conductance spectra of device #2 at different temperatures. Curves are shifted vertically for clarity.

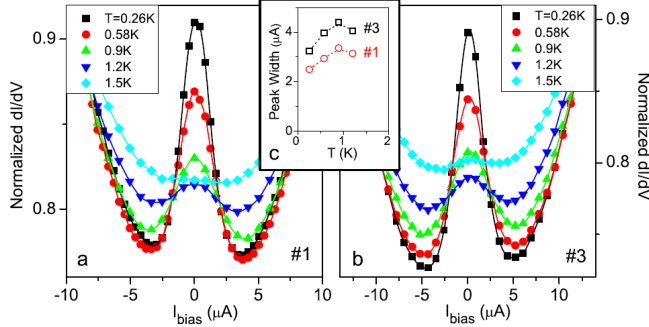


FIG. 5: (color online) Normalized  $dI/dV$  plotted against bias current for devices #1 (a) and #3 (b). (c) Temperature dependence of the full width of the peak at half height, for both devices #1 and #3.

width is controlled by thermal broadening.

### III. COMPARATIVE EXPERIMENT: Sn-GRAPHITE JUNCTIONS

In order to examine whether the conductance anomalies observed in Sn-Bi<sub>2</sub>Se<sub>3</sub> interfacial junctions are intrinsic properties of the interface between an *s*-wave superconductor Sn and a helical metal, we have made two more devices for comparison by replacing Bi<sub>2</sub>Se<sub>3</sub> with bulk

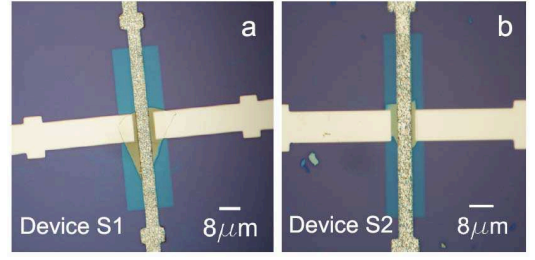


FIG. 6: (color online) Optical images of Sn-graphite devices S1 (a) and S2 (b).

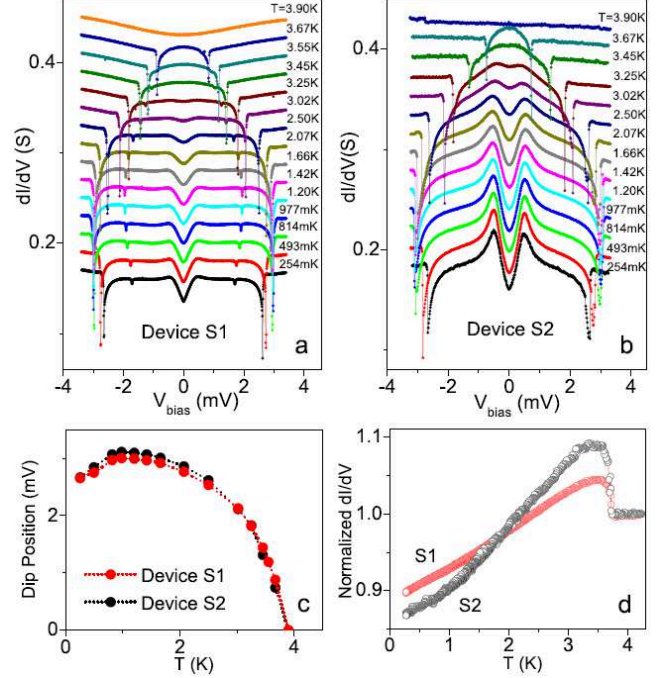


FIG. 7: (color online) Conductance spectra of Sn-graphite devices S1 (a) and S2 (b) taken at different temperatures. Curves are shifted vertically for clarity. (c) Temperature dependencies of the dip positions. (d) Normalized zero bias  $dI/dV$  as a function of temperature.

graphite, while keeping other parameters the same. We choose graphite because it is similar to Bi<sub>2</sub>Se<sub>3</sub> in carrier density and mobility, but with much weaker spin-orbit coupling strength<sup>19</sup>. The two devices, made of graphite flakes of thickness  $\sim 100$  nm, are labeled as S1 and S2, respectively. Their optical images are shown in Fig. 6.

In Fig. 7(d) we show the measured zero-bias differential conductance  $G$  as a function of temperature for these two devices. The data are normalized to their values above  $T_c \approx 3.8$  K (around  $6 \Omega$  for both devices). The  $G - T$  curves are similar to that of the Sn-Bi<sub>2</sub>Se<sub>3</sub> devices, except that there is no upturns below  $\sim 1.2$  K. The conductance decreases with decreasing temperature monotonously down to 250 mK without saturation.

Figures 7(b) and 7(c) show the conductance spectra of device S1 and S2, respectively, taken at different temper-

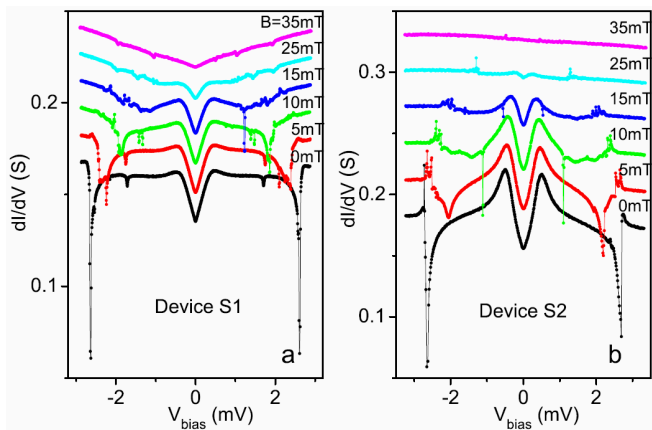


FIG. 8: (color online) Conductance spectra of Sn-graphite devices S1 (a) and S2 (b) taken at 250 mK and in different magnetic fields. Curves are shifted vertically for clarity.

atures. A single gap is developed at low temperatures. The coherence peak of that gap is located at  $\sim 0.5$  mV, which is close to the superconducting gap of the Sn electrode. Neither a zero bias peak nor a second smaller gap was observed. This single gap structure can be well understood within the BTK theory.

There is a sharp dip at each side of the conductance spectrum, beyond which the curve becomes flat and featureless. As discussed in Section II, we attribute the dip structure to the local destruction of superconductivity of the Sn film near the junction. The fact that similar dips were found in both Sn-Bi<sub>2</sub>Se<sub>3</sub> and Sn-graphite junctions suggests that these dips are not specifically related to Bi<sub>2</sub>Se<sub>3</sub>.

The magnetic field dependencies of the conductance spectra of devices S1 and S2 are plotted in Figs. 8(a) and 8(b), respectively. All the structures in the spectrum can be removed by applying a magnetic field higher than the  $H_c$  of Sn, indicating that they are related to the superconductivity of Sn electrode.

In summary, our comparative experiment on Sn-graphite devices reveals only a single-gapped structure, neither a second smaller gap nor a ZBCP was observable, unlike those on Sn-Bi<sub>2</sub>Se<sub>3</sub> devices. The data also show that the non-monotonous temperature dependence of the dip position is irrelevant to the use of Bi<sub>2</sub>Se<sub>3</sub>.

#### IV. DISCUSSION: POSSIBLE ORIGINS OF THE ZBCP AND THE DOUBLE-GAP STRUCTURE

The general trends of the  $G - T$  and  $G - V_{\text{bias}}$  curves of the Sn-Bi<sub>2</sub>Se<sub>3</sub> devices can be understood within the framework of the BTK theory<sup>16</sup>, which was developed in the early 1980's to describe the two-particle process at S-N interfaces. However, this theory cannot explain the appearance of a second gap, nor the ZBCP at low temperatures.

Previously, ZBCPs were also observed in some S-N<sup>20–24</sup> and S-insulator-N<sup>25</sup> junctions, and were explained in several different mechanisms.

The first possible mechanism is related to incoherent accumulation of Andreev reflections (AR), which happens when there is a large probability of backscattering due to, e.g., the involvement of the other surface of the normal-metal thin film<sup>21,22</sup>. ZBCPs of this kind usually grows up immediately below  $T_c$ . The ZBCP observed here seems irrelevant to this mechanism, since it has sensitive  $T$  and  $B$  dependencies, appearing at much lower temperatures.

The second possible mechanism is related to coherent scattering of carriers near the interface due to phase conjugation between the electron's and the hole's trajectories, leading to an enhanced AR probability<sup>26</sup>. This mechanism is also expressed in a more general way by using a random matrix theory<sup>27</sup>. A ZBCP caused by this mechanism is sensitive to both temperature and magnetic field, since it involves a coherent loop. However, these theories do not take account of the strong SOC and its resulting Berry phase. In the presence of strong SOC, the phase accumulated by the incident electron along its path cannot be canceled by the retro-reflected hole, i.e., the phase difference between the  $N^{\text{th}}$  and the  $(N + 1)^{\text{th}}$  reflected hole is not zero. Furthermore, the theory in Ref. [27] suggests that this kind of ZBCP often appear in junctions with relatively strong scattering rate, and that the value of the conductance peak will not exceed the conductance of the normal state, whereas in our experiment the ZBCP can be higher than the conductance of the normal state, as shown in Fig. 1(a) for device #2. Therefore, we believe that the ZBCP observed in our experiments is not caused by the aforementioned constructive interference.

The third explanation is to phenomenologically attribute ZBCP to a pair current flowing between the superconducting electrode and the proximity-induced superconducting phase<sup>20</sup>. For a ZBCP of this type, its behavior will resemble the critical supercurrent of a Josephson junction. As temperature decreases, the critical current of a Josephson junction will first increase then get saturated. For a ZBCP of this type, therefore, its peak width is expected to increase with decreasing  $T$  if it is plotted against bias current. However, the ZBCP in this experiment shrinks with decreasing  $T$ , as can be seen in Fig. 5. Therefore, the pair current picture seems inapplicable to our results.

Another possible mechanism of ZBCP involves unconventional superconductivity with an asymmetric orbital order parameter<sup>28–35</sup>. For example, in the  $p$ -wave superconductor Sr<sub>2</sub>RuO<sub>4</sub>, the reflection of order parameter at the S-N edge in the  $ab$ -plane feels a sign-change, giving rise to an Andreev bound state at the Fermi energy and a ZBCP in tunneling measurement<sup>28</sup>. After having ruled out other possible mechanisms to the best of our knowledge, we believe that this mechanism involving unconventional superconductivity is most likely responsible for the appearance of the ZBCP in this experiment.

Our entire picture for the observed phenomena is as follows. With decreasing  $T$  to below  $T_c$  of Sn, proximity effect develops at the S-N interface via two-particle exchange processes, i.e., Cooper pairs are exchanged from the Sn side to the  $\text{Bi}_2\text{Se}_3$  side, and entangled quasi-particle pairs are exchanged back in a time-reversal process, known as AR. Unlike in an usual proximity effect, where only a single gap of the parent superconductor is seen, the observation of a second gap here indicates the formation of a new S'-N interface where S' is not Sn but a proximity-effect-induced superconducting  $\text{Bi}_2\text{Se}_3$  phase. The original Sn- $\text{Bi}_2\text{Se}_3$  interface becomes an S-S' interface whose role vanishes in resistance measurement, so that the gap structure related to Sn is either absent or largely suppressed. We speculate that the suppression of back-scattering due to strong SOC and the high electron mobility in  $\text{Bi}_2\text{Se}_3$  would help maintaining the coherence of the two-particle AR process in space and time domains, thus stabilizing the proximity-effect-induced new superconducting phase (S'-phase) in a substantially large volume of  $\text{Bi}_2\text{Se}_3$ .

With further decreasing  $T$ , the new superconducting phase becomes uniformly developed, then the coherence peaks at the two shoulders of the gap appear. The ZBCP grows up simultaneously, presumably also related to the improved uniformity of the new superconducting phase at low temperatures.

Since no ZBCP is observed in similar devices made of graphite which has negligible SOC, one would naturally speculate that strong SOC is the cause for generating the ZBCP in Sn- $\text{Bi}_2\text{Se}_3$  devices. The important role of strong SOC to the electron states in  $\text{Bi}_2\text{Se}_3$  has been revealed by the unusually robust behavior of electron weak-anti-localization<sup>10-14</sup>, a phenomenon which mainly occurs in 2D electron systems. It indicates the existence of a Berry phase  $\pi$  in the electrons' band structure. The new superconducting phase inhabited in such a background, with inter-locked momentum and spin degrees of freedom, is believed to own effectively a spinless  $p_x + ip_y$  pairing symmetry. The asymmetric orbital part of the order parameter, inherited from the Berry curvature of the bands, forms resonant bound states at the S'-N interface due

to the interference between the incoming and reflecting waveforms there, hence giving rise to the observed ZBCP. With such a picture, it is natural that the peak width gets narrower with reduced thermal broadening at lower  $T$ .

## V. CONCLUSION

To summarize, we have investigated the conductance spectra of S-N junctions between an  $s$ -wave superconductor Sn and a strong SOC material  $\text{Bi}_2\text{Se}_3$ . A small gap different from that of Sn was clearly resolved, together with a ZBCP growing up at low temperatures. The results indicate the formation of a new superconducting phase with unconventional pairing symmetry at the interface. Our work would encourage future experiments to search for Majorana fermions and other pertinent properties by employing hybrid structures of  $s$ -wave superconductor and topological insulator-related materials.

## Acknowledgments

We would like to thank H. F. Yang and C. Q. Jin for experimental assistance, L. Fu, Z. Fang, X. Dai, Q. F. Sun, X. C. Xie and S. C. Zhang for stimulative discussions. This work was supported by the National Basic Research Program of China from the MOST under the contract No. 2009CB929101 and 2011CB921702, by the NSFC under the contract No. 11174340 and 11174357, and by the Knowledge Innovation Project and the Instrument Developing Project of CAS.

*Note added in reversion:* After the submission of this manuscript, observation of a supercurrent and possible evidence of Pearl vortices were reported in W- $\text{Bi}_2\text{Se}_3$ -W junction<sup>36</sup>, a ZBCP was observed on normal metal- $\text{Cu}_x\text{Bi}_2\text{Se}_3$  point contact<sup>37</sup>, and evidence of perfect Andreev reflection of the helical mode was obtained in InAs/GaSb Quantum Wells<sup>38</sup>.

---

\* Corresponding authors: lilu@iphy.ac.cn

<sup>1</sup> X.-L. Qi and S.-C. Zhang, *Physics Today* **63**, 33 (2010).

<sup>2</sup> M. Z. Hasan and C. L. Kane, *Rev. Mod. Phys.* **82**, 3045 (2010) and references therein.

<sup>3</sup> J. E. Moore, *Nature* **464**, 194-198 (2010) and references therein.

<sup>4</sup> C. J. Bolech and E. Demler, *Phys. Rev. Lett.* **98**, 237002 (2007).

<sup>5</sup> L. Fu and C. L. Kane, *Phys. Rev. Lett.* **100**, 096407 (2008).

<sup>6</sup> L. Fu and C. L. Kane, *Phys. Rev. Lett.* **102**, 216403 (2009).

<sup>7</sup> Y. Tanaka, T. Yokoyama and N. Nagaosa, *Phys. Rev. Lett.* **103**, 107002 (2009).

<sup>8</sup> K. T. Law, P. A. Lee and T. K. Ng, *Phys. Rev. Lett.* **103**, 237001 (2009).

<sup>9</sup> B. Sacépé, J. B. Oostinga, J. Li, A. Ubalini, N. J.G. Couto, E. Giannini and A. F. Morpurgo, arXiv:1101.2352v1 (2011).

<sup>10</sup> J. G. Checkelsky, Y. S. Hor, M.-H. Liu, D.-X. Qu, R. J. Cava, and N. P. Ong, *Phys. Rev. Lett.* **103**, 246601 (2009).

<sup>11</sup> J. Chen, H.-J. Qin, F. Yang, J. Liu, T. Guan, F.-M. Qu, G.-H. Zhang, J.-R. Shi, X.-C. Xie, C.-L. Yang, K.-H. Wu, Y. Q. Li and L. Lu, *Phys. Rev. Lett.* **105**, 176602 (2010).

<sup>12</sup> H.-T. He, G. Wang, T. Zhang, I.-K. Sou, and J.-N. Wang, arXiv:1008.0141 (2010).

<sup>13</sup> M.-H. Liu, C.-Z. Chang, Z.-C. Zhang, Y. Zhang, W. Ruan, K. He, L.-L. Wang, X. Chen, J.-F. Jia, S.-C. Zhang, Q.-K. Xue, X.-C. Ma, and Y.-Y. Wang, arXiv:1011.1055 (2010).

<sup>14</sup> J. Wang, A. M. DaSilva, C.-Z. Chang, K. He, J. K. Jain,

- N. Samarth, X.-C. Ma, Q.-K. Xue, and M. H. W. Chan, arXiv:1012.0271v1 (2010).
- <sup>15</sup> H.-J. Zhang, C.-X. Liu, X.-L. Qi, X. Dai, Z. Fang and S.-C. Zhang, *Nature Phys.* **5**, 438 (2009)
  - <sup>16</sup> G. E. Blonder, M. Tinkham and T. M. Klapwijk, *Phys. Rev. B* **25**, 4515 (1982).
  - <sup>17</sup> See Supplemental Material at [URL inserted by publisher] for supporting data.
  - <sup>18</sup> There is about 10  $\mu$ V of smearing on the ZBCP by the small ac voltage used in the measurement.
  - <sup>19</sup> Y.-G. Yao, F. Ye, X.-L. Qi, S.-C. Zhang, and Z. Fang, *Phys. Rev. B* **75**, 041401(R) (2007).
  - <sup>20</sup> A. Kastalsky, A. W. Kleinsasser, L. H. Greene, R. Bhat, F. P. Milliken and J. P. Harbison, *Phys. Rev. Lett.* **67**, 3026 (1991).
  - <sup>21</sup> C. Nguyen, H. Kroemer and E. L. Hu, *Phys. Rev. Lett.* **69**, 2847 (1992).
  - <sup>22</sup> P. Xiong, G. Xiao and R. B. Laibowitz, *Phys. Rev. Lett.* **71**, 1907 (1993).
  - <sup>23</sup> N. Kim, H.-J. Lee, J.-J. Kim, J.-O. Lee, J. W. Park, K.-H. Yoo, S. Lee, and K. W. Park, *Solid State Commun.* **115**, 29 (2000).
  - <sup>24</sup> N. Agraït, J. G. Rodrigo and S. Vieira, *Phys. Rev. B* **46**, 5814 (1992).
  - <sup>25</sup> A. Vaknin and Z. Ovadyahu, *J. Phys.: Cond. Matter* **9**, L303 (1997).
  - <sup>26</sup> B. J. van Wees, P. de Vries, P. Magnée and T. M. Klapwijk, *Phys. Rev. Lett.* **69**, 510 (1992).
  - <sup>27</sup> C. W. J. Beenakker *Phys. Rev. B* **46**, 12841 (1992).
  - <sup>28</sup> F. Laube, G. Goll, H. v. Löhneysen, M. Fogelström and Lichtenberg, *Phys. Rev. Lett.* **84**, 1595 (2000).
  - <sup>29</sup> L. J. Buchholtz and G. Zwicknagl, *Phys. Rev. B* **23**, 5788 (1981).
  - <sup>30</sup> C. Bruder, *Phys. Rev. B* **41**, 4017 (1990).
  - <sup>31</sup> C. R. Hu, *Phys. Rev. Lett.* **72**, 1526 (1994).
  - <sup>32</sup> M. Yamashiro, Y. Tanaka, and S. Kashiwaya, *Phys. Rev. B* **56**, 7847 (1997).
  - <sup>33</sup> C. Honerkamp and M. Sigrist, *J. Low Temp. Phys.* **111**, 895 (1998).
  - <sup>34</sup> S. Kashiwaya and Y. Tanaka, *Rep. Prog. Phys.* **63**, 1641 (2000).
  - <sup>35</sup> A. Calzolari, D. Daghero, R. S. Gonnelli, G. A. Ummarino, V. A. Stepanov, R. Masini, M. R. Cirnberle and M. Ferretti, *J. Phys. Chem. Solids* **67**, 597 (2006).
  - <sup>36</sup> D.-M. Zhang, J. Wang, A. M. DaSilva, J. S. Lee, H. R. Gutierrez, M. H. W. Chan, J. Jain and N. Samarth, *Phys. Rev. B* **84**, 165120 (2011).
  - <sup>37</sup> S. Sasaki, M. Kriener, K. Segawa, K. Yada, Y. Tanaka, M. Sato, Y. Ando, *Phys. Rev. Lett.* **107**, 217001 (2011).
  - <sup>38</sup> I. Knez, R. Du and G. Sullivan, arXiv:1106.5819v1 (2011).